

The QXS-SAROPT Dataset for Deep Learning in SAR-Optical Data Fusion

Meiyu Huang, Yao Xu, Lixin Qian, Weili Shi, Yaqin Zhang,
Wei Bao, Nan Wang, Xuejiao Liu, Xueshuang Xiang

Abstract—Deep learning techniques have made an increasing impact on the field of remote sensing. However, deep neural networks based fusion of multimodal data from different remote sensors with heterogeneous characteristics has not been fully explored, due to the lack of availability of big amounts of perfectly aligned multi-sensor image data with diverse scenes of high resolution, especially for synthetic aperture radar (SAR) data and optical imagery. In this paper, we publish the QXS-SAROPT dataset to foster deep learning research in SAR-optical data fusion. QXS-SAROPT comprises 20,000 pairs of corresponding image patches, collected from three port cities: San Diego, Shanghai and Qingdao acquired by the SAR satellite GaoFen-3 and optical satellites of Google Earth. Besides a detailed description of the dataset, we show exemplary results for two representative applications, namely SAR-optical image matching and SAR ship detection boosted by cross-modal information from optical images. Since QXS-SAROPT is a large open dataset with multiple scenes of the highest resolution of this kind, we believe it will support further developments in the field of deep learning based SAR-optical data fusion for remote sensing.

Index Terms—Synthetic aperture radar (SAR), optical remote sensing, GaoFen-3, deep learning, data fusion

1 INTRODUCTION

WITH the rapid development of deep learning, remarkable breakthroughs have been made in deep learning-based land use segmentation, scene classification, object detection and recognition on the field of remote sensing in the past decade [1], [2], [3]. This is mainly due to the powerful feature extraction and representation

ability of deep neural networks [4], [5], [6], which can well map the remote sensing observations into the eventually desired geographical knowledge. However, the current mainstream remote sensing image interpretation technology is still mainly focused on mono-modal data, and cannot make full use of the complementary and correlated information of multimodal data from different sensors with heterogeneous characteristics, resulting in insufficient intelligent interpretation capabilities and limited application scenarios. For example, optical imaging based on angular measurements is easily restricted by illumination and weather conditions, based on which accurate interpretation cannot be obtained at night or under complex weather with clouds, fog and so on. Compared with optical imaging, Synthetic Aperture Radar (SAR) imaging can achieve full-time and all-weather earth observations based on range measurements, however, it is difficult

- Meiyu Huang, Yao Xu, Lixin Qian, Weili Shi, Yaqin Zhang, Wei Bao, Nan Wang, Xuejiao Liu, Xueshuang Xiang are with Qian Xuesen Laboratory of Space Technology, China Academy of Space Technology, Beijing, China. E-mail: huangmeiyu@qxslab.cn; xuyao@qxslab.cn; qianlixin@whu.edu.cn; shiweili@qxslab.cn; 493834755@qq.com; baowei97@163.com; 824663747@qq.com; liuxuejiao@qxslab.cn; xiangxueshuang@qxslab.cn
- Meiyu Huang, Yao Xu and Lixin Qian contributed equally to this work.
- Corresponding author: Xueshuang Xiang.

This work is supported by the Beijing Nova Program of Science and Technology under Grant Z191100001119129 and the National Natural Science Foundation of China 61702520.

to interpret the SAR images observing physical properties instead of chemical characteristics (texture features) of the target scene as optical images, even for well-trained experts. Therefore, gathering sufficient amounts of training SAR data with diverse scenes and accurate labeling is a challenging problem, which heavily affects the deep research and application of SAR image based intelligent interpretation.

To address the above issues, one of the most promising directions of deep learning in remote sensing is multimodal data fusion [7], [8], [9], [10], especially for a combined exploitation of SAR and optical data as these data modalities are completely different from each other both in terms of geometric and radiometric appearance [11], [12], [13], [14]. To foster the research of SAR-optical data fusion based on deep learning, it is of utmost importance to have access to big datasets of perfectly aligned images or image patches. However, gathering such a big amount of aligned multi-sensor image data is a non-trivial task that requires quite some engineering efforts [15]. Moreover, the existing SAR-optical patch matching dataset either lacks of scene diversity due to the huge difficulty in building accurate 3D reconstruction models to implement pixel-level matching between optical and SAR images [16], or has a low resolution limited by the remote sensing satellites used for data acquisition [17].

Based on the analysis above, in this paper, we publish the so-called QXS-SAROPT dataset containing multiple scenes of a high resolution of 1 meter. Specifically, it is comprised of 20,000 SAR-optical patch-pairs acquired by the SAR satellite GaoFen-3 [18] and optical satellites used for Google Earth Engine providing an on-going supply of diverse Earth observation satellite data to the end user free-of charge [19]. The patches are collected from locations spread across land masses of San Diego, Shanghai and Qingdao. The source and construction of the dataset, its strengths and limitations, as well as two example applications are described in the rest of this paper.

2 GAOFEN-3 REMOTE SENSING DATA

The Gaofen-3 satellite [18], developed by China Aerospace Science and Technology Corporation, is a part of the Chinese Gaofen (High-Resolution) Earth Observation Project. It is the first C-band and multi-polarization SAR imaging satellite in low earth orbit with a resolution of 1 meter in China.

Equipped with 12 acquisition modes, Gaofen-3 has more working modes compared to other SAR satellites. It not only contains a range of strip-maps, such as the Ultra-fine Strip-Map (UFS), Fine Strip-Map (FSI), Wide Fine Strip-Map (FSII), Standard Strip-Map(SS), Quad-Pol Strip-Map(QPSI), but also has the scanning modes (Narrow ScanSAR and Wide ScanSAR). Further, it can be used in the spotlight, wave, global observation, extended incidence angles imaging modes as well. Accordingly, its imaging resolution varies from 1 meter to 500 meters and its imaging swath ranges from 10 kilometers to 650 kilometers.

For the Gaofen-3 images in our dataset, the spotlight imaging mode with the highest resolution is used. During the SAR imaging process, the antenna performs beam scanning in the azimuth direction to increase the synthetic aperture time and to obtain a higher azimuth resolution compared to the strip mode. The azimuth scanning angle is $\pm 1.9^\circ$, and an active phased array antenna is used to achieve continuous scanning of the azimuth beam. The 240MHz bandwidth is used to meet the requirement of high resolution of 1 meter.

3 CONSTRUCTION OF THE QXS-SAROPT DATASET

The procedure for the dataset construction is shown in Figure 1. In detail, it comprises the following steps:

3.1 Selecting SAR images

Our SAR data originate from the spotlight mode images of Gaofen-3 with single polarization, provided by CRESDA (China Centre for Resource Satellite Data and Application). For application scenarios such as land cover segmentation, scene

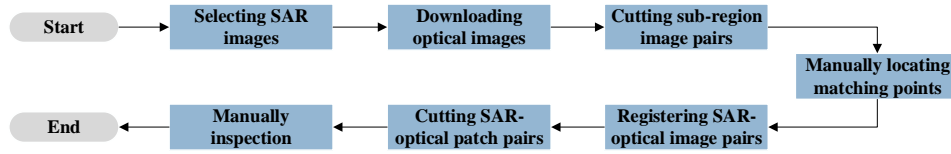


Fig. 1. Flowchart of the procedure for construction of QXS-SAROPT.

classification, ship detection and recognition, we first select three SAR images acquired by the Gaofen-3 satellite that contain rich land cover types such as inland, offshore, and mountains. The ground resolution of the SAR images is 1 meter. The area of each image is 100 square kilometers from three big port cities: San Diego, Shanghai, Qingdao. Image sizes are 14624×33820 , 17080×28778 , and 17080×28946 respectively. Details of these images, including resolution, swath, incidence angle, and polarization are presented in Table 1. The coverage of these images is shown in Figure 2.

3.2 Downloading corresponding optical images

We then download the optical images of the corresponding area with a ground resolution of 1 meter from Google earth using the cloud-based remote sensing platform Google Earth Engine [19], which provides an extensive data catalogue containing several petabytes of remote sensing imagery and other freely available geodata. Given the latitude and longitude coordinates of the desired area and the specified resolution, the corresponding optical images are selected and downloaded, from which we have later extracted our optical image patch.

3.3 Cutting SAR-optical image pairs into sub-region image pairs

Optical imagery reflects the chemical characteristics of the scene and follows a perspective imaging geometry, while SAR imagery collects information about the physical properties of the scene and follows a range-based imaging geometry. Therefore, the optical image is totally different from the SAR image, which makes it impossible

to accurately register the whole optical image with the whole corresponding SAR image [20]. To address the above issue, we cut the whole SAR-optical image pair into several sub-region image pairs according to the complexity of land coverage. After that, we can register the sub-region image pairs separately instead of directly registering the whole image pair.

3.4 Manually locating matching points of sub-region SAR-optical image pairs

As mentioned above, the optical image and SAR image are completely different from each other both in terms of geometric and radiometric appearance due to different imaging mechanism. Therefore, it is not advisable to register them directly by matching points located automatically by the existing image registration approaches [21] mainly designed for registering optical images. In order to cope with the strongly different geometric and radiometric appearances of SAR and optical imagery, we manually locate the matching point of the sub-region SAR-optical image pairs. The matching points are selected as the corner points of buildings, ships, roads, etc. Figure 3 shows matching points manually selected for one exemplary sub-region SAR-optical image pair.

3.5 Registering sub-region SAR-optical image pairs

With the manually located matching points, we then use an existing automatic image registration software to register the sub-region SAR-optical image pairs by leveraging various interpolation methods, such as Bilinear, Nearest Neighbor and Cubic Convolution interpolation. Here, we take the SAR image as the reference image and the optical image as the registration image. Figure 4

TABLE 1
Detailed information of the SAR images of Gaofen-3 for constructing QXS-SAROPT.

No	Coverage region	Imaging mode	Resolution Rg. \times Az.(m)	Swath (km)	Incident Angle ($^{\circ}$)	Polarization	Image size
1	San Diego	spotlight	1	10	20 $^{\circ}$ 50	single	14624 \times 33820
2	Shanghai						17080 \times 28778
3	Qingdao						17080 \times 28946



Fig. 2. Image coverage of Gaofen-3. The red rectangles indicate the coverage of each image.

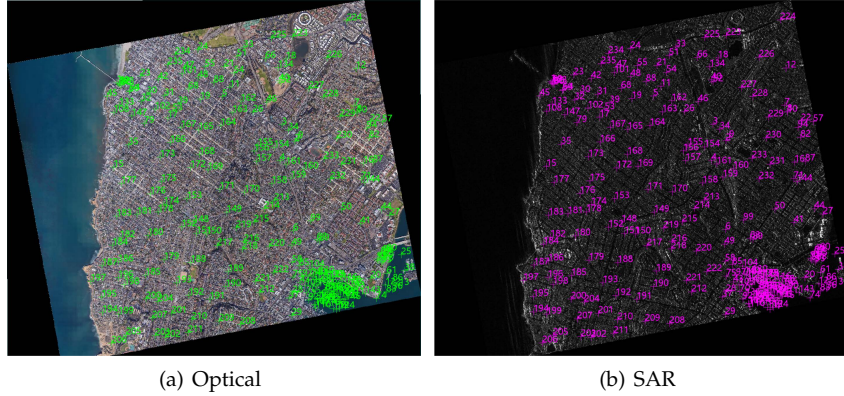


Fig. 3. Illustration of matching points manually selected for one exemplary sub-region SAR-optical image pair.

shows an example of registered sub-region SAR-optical image pair.

3.6 Cutting registered sub-region SAR-optical image pairs into patch-pairs

Since our goal is to construct a dataset of patch-pairs that can be used to train deep learning models for various SAR-optical data fusion tasks,

the registered sub-region SAR-optical image pairs are then cropped into small patches of 256 \times 256 pixels. Using a stride of 52, we reduce the overlap between neighboring patches to only 20% while maximizing the number of independent patches we can get out of the available scenes. We end up with 46071 Gaofen-3/GoogleEarth patch-pairs after this step.

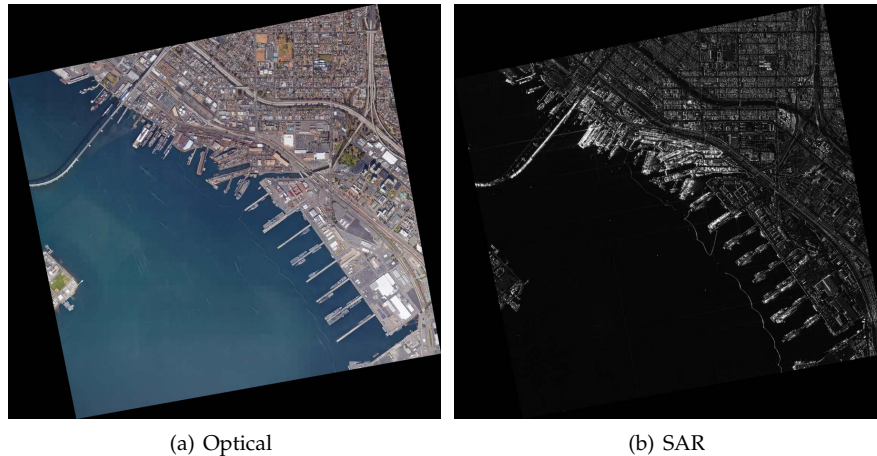


Fig. 4. Illustration of a exemplary registered sub-region SAR-optical image pair.

3.7 Manual inspection

In order to remove similar or sub-optimal patches that, e.g., contain only texture-less sea area or visible mosaicking seamlines, we have inspected all patches visually. In this step, 26071 patch-pairs are manually removed, leaving the final amount of 20,000 quality-controlled patch-pairs. Some examples are shown in Figure 5

4 DATASET AVAILABILITY

The QXS-SAROPT dataset is shared under the open access license CCBY and available for download at <https://github.com/yaoxu008/QXS-SAROPT>. This paper must be cited when the dataset is used for research purposes.

5 EXAMPLE APPLICATIONS

In this section, we present two example applications, for which the dataset has been used already, including SAR-optical image matching and SAR ship detection. These should serve as inspiration for future use cases and ignite further research on deep learning-based SAR-optical data fusion.

5.1 SAR-optical image matching

Image matching of multi-modal data remains challenging to this day, because well-established

methods strive to measure similarity between mono-modal imagery. Specifically, the matching of SAR and optical images is more difficult due to the different imaging geometry [22], [23], [24], [25], [26]. The QXS-SAROPT dataset can assist in creating solutions in the field of SAR-optical image matching by providing the large quantities of data required to exploit modern deep matching approaches, such as proposed by [27]: Using a bridge neural network (BNN) [28] architecture, corresponding SAR-optical image patches of the QXS-SAROPT dataset can be projected into a common feature subspace where similarities can be easily measured. The matching accuracy of a test subset can reach 82.9% and 82.8% with the model of [27] trained on 70% patch-pairs of the QXS-SAROPT dataset using the ResNet50 [6] and Darknet53 [29] backbone, respectively. The detailed results can be seen in Table 2, and some exemplary matches correctly identified for the test subset are shown in Figure 6.

TABLE 2
Results for BNN [28] patch-matching trained on QXS-SAROPT.

Backbone	Accuracy	Precision	Recall
ResNet50 [6]	0.829	0.748	0.993
Darknet53 [29]	0.828	0.746	0.995



Fig. 5. Some exemplary patch-pairs from the QXS-SAROPT dataset. Top part: Google Earth RGB image patches, bottom part: GaoFen-3 SAR image patches.

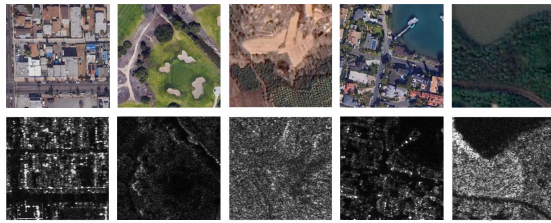


Fig. 6. Some correctly identified matching patch-pairs by BNN [28] for a test subset of QXS-SAROPT. Top row: optical images, bottom row: corresponding SAR images.

5.2 SAR ship detection

SAR ship detection in complex scenes is a great challenging task. Because of powerful feature embedding ability, convolutional neural networks (CNN) [4]-based SAR ship detection methods have drawn considerable attention. The pretraining technique is usually adopted to support these CNN-based SAR ship detectors due to the scarce labeled SAR images. However directly leveraging ImageNet [30] pretraining is hardly to obtain a good ship detector because of different imaging geometry between optical and SAR images. The QXS-SAROPT dataset can provide solutions for SAR ship detection, such as [27] proposing an optical-SAR matching (OSM) pretraining technique to enhance the general feature embedding of SAR images by BNN [28] based on the QXS-SAROPT dataset. BNN can transfer plentiful tex-

ture features from optical images to SAR images and the SAR CNN can be further used as the backbone of the detection framework to perform SAR ship detection. The overall process to implement SAR ship detection using BNN based on the QXS-SAROPT dataset is depicted in 7. As shown in Table 3, compared to ImageNet pretraining based SAR ship detector (ImageNet-SSD), the Average Precision (AP) of detection results of OSM pretraining based SAR ship detector (OSM-SSD) on SAR ship detection dataset AIR-SARShip-1.0 [31] can be improved by 1.32% and 1.24% using two-stage detection benchmark: Faster R-CNN [32] and one-stage detection benchmark: YOLOv3 [29], respectively. For more detailed results, please refer to [27].

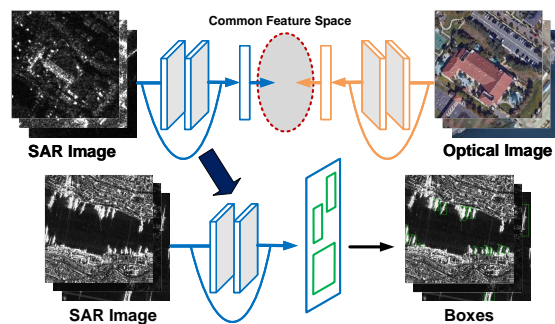


Fig. 7. The overall process to implement SAR ship detection using BNN [28] based on the QXS-SAROPT dataset.

TABLE 3
SAR ship detection results on AIR-SARShip-1.0 [31]
using ImageNet-SSD pretrained on ImageNet and
OSM-SSD pretrained on QXS-SAROPT.

	Faster R-CNN [32]	YOLOv3 [29]
ImageNet-SSD	0.8720	0.8712
OSM-SSD	0.8852	0.8836

6 STRENGTHS AND LIMITATIONS OF THE DATASET

To our knowledge, QXS-SAROPT is the first dataset providing very-high-resolution (1m) co-registered SAR and optical satellite image patches spread over three big port cities in the world. The other two existing datasets in this domain are the so-called SARoptical dataset published by [16] and the SEN1-2 dataset published by [17]. In contrast to the QXS-SAROPT dataset, SARoptical provides very-high-resolution image patches from TerraSAR-X and aerial hotogrammetry based on a deterministic alignment of SAR and optical imagery via previously reconstructed and subsequently co-registered 3D point clouds, but is restricted to a mere 10,000 patches extracted from a single scene containing only inland area focusing on urban buildings, which is possibly not sufficient for many deep learning applications—especially since many patches show an overlap of more than 50% and the whole size of each patch is only 112×112 . With its 20,000 patch-pairs extracted from multiple scenes containing inland area, sea area and mountain area focusing on not only buildings but also harbours, ships and so forth, QXS-SAROPT will thus be a valuable data source for many researchers in the field of SAR-optical data fusion and remote sensing-oriented deep learning. A particular advantage is that the dataset can easily be used for scene classification because it covers a variety of land types.

Regarding SEN1-2, it is the largest dataset of this kind with 282,384 pairs of corresponding image patches spread over the whole globe and all meteorological seasons. However, it is built on Sentinel-2 data with a low resolution down to 5m, which may be not applicable for feature learning of small-sized objects, such as

small ships. Conversely, QXS-SAROPT can well enhance the feature learning ability of small-sized objects because of the high resolution of GaoFen-3.

However, also QXS-SAROPT does not come without limitations: For example, it only covers three port cities now, which is still limited in both coverage and scenes. Furthermore, at the time we carried out the dataset preparation, we fixed the patch size as 256×256 , which may be not suitable for different applications. We are planning to extend the dataset for a future version 2 release accordingly.

7 SUMMARY AND CONCLUSION

In this paper, we have described and released the QXS-SAROPT dataset, which contains 20,000 pairs of SAR and optical image patches extracted from multiple GaoFen-3 and Google Earth scenes of a very high resolution. We assume this dataset will foster the development of deep learning approaches in the field of SAR-optical data fusion of satellite remote sensing. In the future, we plan on releasing a refined, second version of the dataset, which covers more land areas with versatile scenes and has different sized patch-pairs suitable for various SAR-optical data fusion tasks.

REFERENCES

- [1] L. Zhang, L. Zhang, and B. Du, "Deep learning for remote sensing data: A technical tutorial on the state of the art," *IEEE Geoscience and Remote Sensing Magazine*, vol. 4, no. 2, pp. 22–40, 2016.
- [2] X. X. Zhu, D. Tuia, L. Mou, G.-S. Xia, L. Zhang, F. Xu, and F. Fraundorfer, "Deep learning in remote sensing: A comprehensive review and list of resources," *IEEE Geoscience and Remote Sensing Magazine*, vol. 5, no. 4, pp. 8–36, 2017.
- [3] G. Tsagkatakis, A. Aidini, K. Fotiadou, M. Giannopoulos, A. Pentari, and P. Tsakalides, "Survey of deep-learning approaches for remote sensing observation enhancement," *Sensors*, vol. 19, no. 18, p. 3929, 2019.
- [4] T. N. Sainath, A.-r. Mohamed, B. Kingsbury, and B. Ramabhadran, "Deep convolutional neural networks for lvcsr," in *2013 IEEE international conference on acoustics, speech and signal processing*. IEEE, 2013, pp. 8614–8618.
- [5] K. Simonyan and A. Zisserman, "Very deep convolutional networks for large-scale image recognition," *arXiv preprint arXiv:1409.1556*, 2014.

- [6] K. He, X. Zhang, S. Ren, and J. Sun, "Deep residual learning for image recognition," in *Proc. CVPR*, 2016, pp. 770–778.
- [7] Michael, Schmitt, Xiao, Xiang, and Zhu, "Data fusion and remote sensing: An ever-growing relationship," *IEEE Geoscience and Remote Sensing Magazine*, vol. 4, no. 4, pp. 6–23, 2016.
- [8] Z. Zhang, G. Vosselman, M. Gerke, C. Persello, D. Tuia, and M. Y. Yang, "Detecting building changes between airborne laser scanning and photogrammetric data," *Remote sensing*, vol. 11, no. 20, p. 2417, 2019.
- [9] Z. Zhang, G. Vosselman, M. Gerke, D. Tuia, and M. Y. Yang, "Change detection between multimodal remote sensing data using siamese cnn," *arXiv preprint arXiv:1807.09562*, 2018.
- [10] P. Feng, Y. Lin, J. Guan, Y. Dong, G. He, Z. Xia, and H. Shi, "Embranchment cnn based local climate zone classification using sar and multispectral remote sensing data," in *IGARSS 2019-2019 IEEE International Geoscience and Remote Sensing Symposium*. IEEE, 2019, pp. 6344–6347.
- [11] S. C. Kulkarni and P. P. Rege, "Pixel level fusion techniques for sar and optical images: A review," *Information Fusion*, vol. 59, pp. 13–29, 2020.
- [12] M. Schmitt, F. Tupin, and X. X. Zhu, "Fusion of sar and optical remote sensing data—challenges and recent trends," in *2017 IEEE International Geoscience and Remote Sensing Symposium (IGARSS)*. IEEE, 2017, pp. 5458–5461.
- [13] X. Li, L. Lei, Y. Sun, M. Li, and G. Kuang, "Multimodal bilinear fusion network with second-order attention-based channel selection for land cover classification," *IEEE Journal of Selected Topics in Applied Earth Observations and Remote Sensing*, vol. 13, pp. 1011–1026, 2020.
- [14] Q. Feng, J. Yang, D. Zhu, J. Liu, H. Guo, B. Bayartungalag, and B. Li, "Integrating multitemporal sentinel-1/2 data for coastal land cover classification using a multibranch convolutional neural network: A case of the yellow river delta," *Remote Sensing*, vol. 11, no. 9, p. 1006, 2019.
- [15] Y. Wang and X. X. Zhu, "The challenge of creating the sarptical dataset," in *IGARSS 2019-2019 IEEE International Geoscience and Remote Sensing Symposium*. IEEE, 2019, pp. 5714–5717.
- [16] —, "The sarptical dataset for joint analysis of sar and optical image in dense urban area," in *IGARSS 2018-2018 IEEE International Geoscience and Remote Sensing Symposium*. IEEE, 2018, pp. 6840–6843.
- [17] M. Schmitt, L. H. Hughes, and X. X. Zhu, "The sen1-2 dataset for deep learning in sar-optical data fusion," *arXiv preprint arXiv:1807.01569*, 2018.
- [18] Q. Zhang, "System design and key technologies of the gf-3 satellite," *Acta Geodaetica et Cartographica Sinica*, vol. 46, no. 3, pp. 269–277, 6 2017.
- [19] N. Gorelick, M. Hancher, M. Dixon, S. Ilyushchenko, and R. Moore, "Google earth engine: Planetary-scale geospatial analysis for everyone," *Remote Sensing of Environment*, vol. 202, 2017.
- [20] Y. Xiang, F. Wang, L. Wan, N. Jiao, and H. You, "Osflo: A robust algorithm for dense optical and sar image registration," *IEEE Transactions on Geoscience and Remote Sensing*, vol. 57, no. 9, pp. 6335–6354, 2019.
- [21] B. Zitová and J. Flusser, "Image registration methods: a survey," *IMAGE AND VISION COMPUTING*, vol. 21, pp. 977–1000, 2003.
- [22] L. Mou, M. Schmitt, Y. Wang, and X. X. Zhu, "A cnn for the identification of corresponding patches in sar and optical imagery of urban scenes," in *2017 Joint Urban Remote Sensing Event (JURSE)*. IEEE, 2017, pp. 1–4.
- [23] L. H. Hughes, M. Schmitt, L. Mou, Y. Wang, and X. X. Zhu, "Identifying corresponding patches in sar and optical images with a pseudo-siamese cnn," *IEEE Geoscience and Remote Sensing Letters*, vol. 15, no. 5, pp. 784–788, 2018.
- [24] L. H. Hughes, D. Marcos, S. Lobry, D. Tuia, and M. Schmitt, "A deep learning framework for matching of sar and optical imagery," *ISPRS Journal of Photogrammetry and Remote Sensing*, vol. 169, pp. 166–179, 2020.
- [25] W. Xiong, Z. Xiong, Y. Zhang, Y. Cui, and X. Gu, "A deep cross-modality hashing network for sar and optical remote sensing images retrieval," *IEEE Journal of Selected Topics in Applied Earth Observations and Remote Sensing*, vol. 13, pp. 5284–5296, 2020.
- [26] Y. Zhang, W. Zhou, and H. Li, "Retrieval across optical and sar images with deep neural network," in *Pacific Rim Conference on Multimedia*. Springer, 2018, pp. 392–402.
- [27] W. Bao, M. Huang, Y. Zhang, Y. Xu, X. Liu, and X. Xiang, "Boosting ship detection in sar images with complementary pretraining techniques," 2021.
- [28] Y. Xu, X. Xiang, and M. Huang, "Task-driven common representation learning via bridge neural network," in *Proceedings of the AAAI Conference on Artificial Intelligence*, vol. 33, 2019, pp. 5573–5580.
- [29] J. Redmon and A. Farhadi, "Yolov3: An incremental improvement," *arXiv preprint arXiv:1804.02767*, 2018.
- [30] O. Russakovsky, J. Deng, H. Su, J. Krause, S. Satheesh, S. Ma, Z. Huang, A. Karpathy, A. Khosla, M. Bernstein, A. C. Berg, and F.-F. Li, "Imagenet large scale visual recognition challenge," *Proc. IJCV*, vol. 115, no. 3, pp. 211–252, 2015.
- [31] S. Xian, W. Zhirui, S. Yuanrui, D. Wenhui, Z. Yue, and F. Kun, "Air-sarship-1.0: High resolution sar ship detection dataset," *J. Radars*, vol. 8, no. 6, pp. 852–862, 2019.
- [32] S. Ren, K. He, R. Girshick, and J. Sun, "Faster r-cnn: Towards real-time object detection with region proposal networks," in *Proc. NIPS*, 2015, pp. 91–99.